Magnetic dipole transitions in $4d^N$ configurations of tungsten ions

V. Jonauskas,* R. Kisielius, A. Kynienė, and S. Kučas
Institute of Theoretical Physics and Astronomy, Vilnius University, A. Goštauto 12, LT-01108 Vilnius, Lithuania

P. H. Norrington
Department of Applied Mathematics and Theoretical Physics, Queen's University of Belfast, Belfast BT7 1NN, Northern Ireland, United Kingdon

(Received 8 July 2009; published 25 January 2010)

Magnetic dipole transitions between the levels of ground $4d^N$ configurations of tungsten ions were analyzed by employing a large basis of interacting configurations. Previously introduced configuration interaction strength between two configurations was used to determine the configurations with the largest contribution to wave functions of atomic states for the considered configurations. Collisional-radiative modeling was performed for the levels of the ground configuration coupled through electric dipole transitions with $4p^5 4d^{N+1}$ and $4d^{N-1}4f$ configurations. New identification of some lines observed in the electron-beam ion trap plasma was proposed based on calculations in which wavelength convergence was reached.

DOI: 10.1103/PhysRevA.81.012506 PACS number(s): 31.15.am, 32.70.Fw, 52.40.Mj

I. INTRODUCTION

Tungsten, due to its low sputtering yield while interacting with plasma particles, is planned to be used in future large fusion devices such as ITER and DEMO. However, some tungsten ions manage to penetrate into the inner core of plasma, and their radiation threatens to terminate ignition of the fusion reaction. It was suggested [1] that the relative abundance of tungsten impurities must not to exceed 10^{-4} for a reactor to perform successfully. Therefore, the spectroscopy of the tungsten ion lines is crucial for exploring the conditions in tokamak plasma.

Although the forbidden transition probabilities are several orders of magnitude weaker than those of the electric dipole ($E1$) transitions, they play an important role in plasma diagnostics because the intensities of the radiation are often very sensitive to electron temperature and density and other plasma parameters. The advantages of forbidden transitions are widely used to study the spectra of astrophysical or laboratory-made plasmas. However, such spectra contain a large number of lines emitted by various ions and elements residing at the line of sight of measurement. Therefore, the wavelengths of lines registered in plasma spectra must be known with high confidence from calculations or experiment. Electron-beam ion trap (EBIT) spectroscopy makes it possible to observe spectra of various ions in a single ionization stage while the adjacent ions are often present in small amounts.

Recently tungsten spectra corresponding to magnetic dipole transitions in $4p^6 4d^N$ ($N = 1, \ldots, 9$) configurations were registered at the Berlin EBIT [2,3]. These measurements included a wide range of wavelengths covering the region from 5 to 1000 Å. The collisional-radiative modeling (CRM) applied in that work used HULLAC codes [4] to identify the observed lines for tungsten ions with charge states $q = 25$–45. A small number of interacting configurations (only six) were used in that study. Deviations of up to 3% from experimental values were obtained for some wavelengths of magnetic dipole ($M1$) transitions between levels of the $4p^6 4d^N$ configurations.

The purpose of the present work is to extend configuration interaction (CI) bases for $4d^N$ ($N = 1, \ldots, 9$) configurations by using the CI strength to determine admixed configurations. The relativistic approach is used to calculate wavelengths and radiative transition probabilities of $M1$ transitions in the $4p^6 4d^N$ ($N = 1, \ldots, 9$) configurations of tungsten ions. The main tool used for this purpose is the Flexible Atomic Code (FAC) from [5,6]. Calculations using the General Purpose Relativistic Atomic Structure Program (GRASP0) [7] are performed using a smaller CI basis in order to cross-check the atomic data obtained with FAC. Recently, FAC was successfully applied for the analysis of the allowed and forbidden transitions for wavelengths between 3 and 10 Å of the Ni-like W^{46+} and Cu-like W^{45+} ions [8] and for the lines of ions W^{39+} to W^{47+} in the range 120–200 Å [9] and spectra from the highly charged tungsten ions W^{54+} to W^{63+} (40–200 Å) [10]. Likewise, the GRASP code was used to calculate wavelengths of the charge states of W^{39+} to W^{45+} in [11].

Previous investigation of tungsten spectra from EBIT plasma demonstrated that the ground level of the considered ion is the most populated [12]. The plane-wave Born approximation is applicable for the energies of electrons used in EBIT measurements, suggesting that the collision rates are proportional to the corresponding radiative transition rates. However, in the present work we have applied CRM to obtain line intensities by solving the rate matrix that includes excitation (de-excitation) by electrons and radiative decay. This provides additional criteria for line selection in the cases in which the calculated wavelengths and $M1$ transition probabilities do not provide conclusive identification.

In Sec. II we discuss our method to choose the basis of configurations that are used to obtain the atomic wave functions in the CI approximation. The CI strength is employed to select strongly interacting configurations, which are further included in the wavelength calculation. Theoretical wavelength values determined on various CI bases are compared with the observed wavelengths in Sec. III. The line identification based

*V.Jonauskas@itpa.lt

on both CI calculation and CRM of the $M1$ line intensities is proposed for the ions W^{29+} through W^{37+}.

II. CONFIGURATION INTERACTION BASIS

Correlation effects have to be taken into account to define the influence of the correlated movement of electrons on the total energy of system. In the widely used CI method, the configurations that have the strongest mixing with the considered configurations are analyzed. The most common way to determine these strongly mixing configurations is to calculate the Hamiltonian matrix, to diagonalize it, and to include in the atomic wave functions only the configurations with expansion coefficients that meet some defined criteria for the consequent calculations. Quite often it is not possible to check a complete set of configurations in this way all at once because the Hamiltonian matrix is too large to be processed with standard computer memory. For this reason the described procedure must be repeated until all important configurations are included to form the set of interacting configurations.

Our approach is based on the method of global characteristics [13] where the energy levels of a configuration are described in their entirety. Therefore, the configurations are described using the average energy of levels, the variance (width), and the skewness (asymmetry) [14–16]. Consequently, all processes among the levels of two configurations are represented by one process between the configurations [17–19]. Using this method, the number of transitions is significantly reduced, and the data can be calculated for tasks that were previously unresolvable. This approach is applicable in cases where transitions take place among several hundreds or even thousands of levels and when the spectral lines coalesce to form unresolved transition arrays [20].

In this work, the method of global characteristics is applied to estimate CI effects in atoms by introducing the CI strength, $T(K, K')$ [15,21]:

$$T(K, K') = \frac{\sum_{\gamma\gamma'} \langle K\gamma|H|K'\gamma'\rangle^2}{\bar{E}(K, K')^2}. \tag{1}$$

The quantity in the numerator of Eq. (1) is the interconfiguration matrix element of the Hamiltonian H and $\bar{E}(K, K')$ is the energy distance between the interacting levels of configurations K and K':

$$\bar{E}(K, K') = \frac{\sum_{\gamma\gamma'} (\langle K\gamma|H|K\gamma\rangle - \langle K'\gamma'|H|K'\gamma'\rangle)\langle K\gamma|H|K'\gamma'\rangle^2}{\sum_{\gamma\gamma'} \langle K\gamma|H|K'\gamma'\rangle^2}. \tag{2}$$

The summation in Eqs. (1) and (2) is performed over all states γ and γ' of both configurations.

Equation (1) is based on the idea that, in the lowest order of the perturbation theory, the interaction between two levels is proportional to the absolute value of the Hamiltonian matrix element between these levels and inversely proportional to the energy difference between them. The CI strength $T(K, K')$ is used as a measure of CI between two configurations. The $T(K, K')$ value, divided by the number of levels of the configuration that interact with the levels of the other configuration, has approximately the meaning of the square of the expansion coefficient at the wave function of the latter configuration in the expansion of the wave function of the former configuration.

The CI strength $T(K, K')$ has been calculated between the considered $4d^N$ configuration and several hundreds of configurations differing from it by states of one or two electrons. All one- and two-electron excitations from the $n = 3$ complex have been included to study their influence. The one-electron excitations are taken up to the $n = 7$ complex while the two-electron excitations include only the $n = 4$ and $n = 5$ complexes. Consequently, a set of configurations has been selected according to the largest values of $T(K, K')$. Calculations were performed using the Dirac-Fock wave functions obtained with the GRASP92 package [22]. The calculated CI strengths between the relativistic configurations were summed afterward to obtain the CI strengths for their nonrelativistic counterparts. The same approach of finding the CI basis has been successfully applied for the $4p^5 4d^{N+1} + 4p^6 4d^{N-1} 4f \rightarrow 4p^6 4d^N$ transitions in W^{30+}. It has enabled us to achieve agreement with the experimental wavelength within error bars [23] whereas previous calculations [24] have produced deviations up to 2 Å. The extended CI basis found from the CI strength has helped explain the discrepancies between previous calculations and measurements [25] for the nondipole $3p \rightarrow 2p$ transitions in solid cobalt, nickel, and copper. It should be mentioned that a similar approach based on second-order perturbation theory was realized earlier for the nonrelativistic configurations [26].

Table I presents the calculated CI strengths between the $4d^N$ configuration and configurations having the largest value of $T(K, K')$. The numbers of configurations are used afterward to describe which sets of configurations are included in our CI list of calculations for the particular wavelengths. It is impossible to include all these configurations in our calculations because the number of configuration state functions (CSFs) increases significantly and would overrun the available computing facilities. For example, the number of CSFs with total angular quantum momentum $J = 5/2$ used in our calculations amounts to 43,018 for the W^{33+} ion. Therefore, the different extended CI bases are used even for various transitions in the same ions because the number of CSFs for some J values significantly increases, and the corresponding Hamiltonian matrices do not fit into computer memory. Moreover, our approach does not allow the particular CSFs that interact weakly or do not interact at all with the active CSF of the considered configuration to be distinguished, which would allow the CI basis to be reduced significantly. The CI strength $T(K, K')$ is summed over the CSFs of configurations and therefore one can expect some deviation from the actual mixing of two CSFs.

We see that three configurations, namely $4p^6 4d^{N-2} 4f^2$, $4p^4 4d^{N+2}$, and $4p^5 4d^N 4f$, which have been already included in previous calculations [3] are also presented in Table I. However, some other configurations, such as $4p^4 4d^N 4f^2$ and $4s4p^5 4d^{N+1} 4f$, demonstrate strong mixing with the considered $4d^N$ configuration. It is interesting that the $4d^{N-1} 5s$ configuration, which was included in previous calculations [2,3], has a low $T(K, K')$ value (W^{29+}: 8.8×10^{-6}, W^{30+}: 5.6×10^{-5}, W^{31+}: 1.8×10^{-4}, W^{32+}: 3.1×10^{-4}, W^{33+}: 3.3×10^{-4}, W^{34+}: 2.1×10^{-4}, W^{35+}: 7.1×10^{-5}, W^{36+}:

TABLE I. CI strengths $T(K, K')$ calculated for the $4d^N$ ($N = 1, \ldots, 9$) configurations of tungsten ions.

	$4d^9$	$4d^8$	$4d^7$	$4d^6$	$4d^5$	$4d^4$	$4d^3$	$4d^2$	$4d^1$
$4d^{-2}4f^2$	1.81(−1)	6.48(−1)	1.34(−0)	1.72(−0)	1.43(−0)	7.37(−1)	2.18(−1)	2.82(−2)	
$4p^{-1}4f$	3.91(−2)	3.16(−1)	1.13(−0)	2.29(−0)	2.92(−0)	2.38(−0)	1.21(−0)	3.54(−1)	4.52(−2)
$4d^{-1}5d$	1.67(−2)	1.14(−1)	3.31(−1)	5.32(−1)	5.05(−1)	2.77(−1)	7.60(−2)	6.33(−3)	8.32(−4)
$4p^{-2}4f^2$	7.39(−3)	3.36(−2)	9.08(−2)	1.61(−1)	1.96(−1)	1.66(−1)	9.61(−2)	3.66(−2)	8.25(−3)
$4p^{-1}5p$	6.29(−3)	4.95(−2)	1.71(−1)	3.37(−1)	4.15(−1)	3.28(−1)	1.62(−1)	4.55(−2)	5.62(−3)
$3d^{-1}4d^{-1}4f^2$	5.31(−3)	2.16(−2)	5.15(−2)	7.89(−2)	8.05(−2)	5.47(−2)	2.39(−2)	6.06(−3)	6.84(−4)
$4p^{-1}4d^{-1}4f\,5g$	4.89(−3)	2.06(−2)	5.09(−2)	8.05(−2)	8.43(−2)	5.87(−2)	2.61(−2)	6.77(−3)	7.76(−4)
$4p^{-2}4d^{+2}$		1.46(−2)	1.18(−1)	4.15(−1)	8.37(−1)	1.05(−0)	8.51(−1)	4.29(−1)	1.24(−1)
$4p^{-1}4d^{-1}5p\,5d$	2.46(−3)	1.02(−2)	2.36(−2)	3.53(−2)	3.21(−2)	2.33(−2)	9.94(−3)	2.47(−3)	2.73(−4)
$4d^{-1}6d$	2.30(−3)	1.41(−2)	4.01(−2)	6.31(−2)	5.88(−2)	3.17(−2)	8.56(−3)	7.02(−4)	8.91(−5)
$4p^{-1}4d^{-1}4f\,6g$	2.29(−3)	8.55(−3)	2.01(−2)	3.03(−2)	3.02(−2)	2.01(−2)	8.53(−3)	2.11(−3)	2.31(−4)
$4s^{-1}4d^{-1}4f^2$	2.23(−3)	9.01(−3)	2.13(−2)	3.24(−2)	3.29(−2)	2.22(−2)	9.64(−3)	2.44(−3)	2.75(−4)
$4d^{-2}5d^2$	2.22(−3)	8.02(−3)	1.59(−2)	1.97(−2)	1.56(−2)	7.75(−3)	2.19(−3)	2.72(−4)	
$4s^{-1}5s$	1.49(−3)	1.17(−2)	4.07(−2)	8.05(−2)	9.95(−2)	7.87(−2)	3.90(−2)	1.10(−2)	1.36(−3)
$4p^{-1}4d^{-1}4f\,7g$	1.34(−3)	4.11(−3)	9.40(−3)	1.38(−2)	1.34(−2)	8.68(−3)	3.60(−3)	8.68(−4)	9.29(−5)
$3d^{-2}4f^2$	1.29(−3)	6.05(−3)	1.68(−2)	3.06(−2)	3.81(−2)	2.74(−2)	1.95(−2)	7.54(−3)	1.73(−3)
$4d^{-2}5d\,6d$	1.16(−3)	3.82(−3)	7.51(−3)	9.24(−3)	7.28(−3)	3.58(−3)	1.01(−3)	1.24(−4)	
$4p^{-1}4d^{-1}4f\,5d$	1.08(−3)	4.35(−3)	9.48(−3)	1.32(−2)	1.23(−2)	7.62(−3)	3.02(−3)	6.99(−4)	7.15(−5)
$3d^{-1}4d^{-1}4f\,5f$	1.06(−3)	4.09(−3)	9.64(−3)	1.46(−2)	1.47(−2)	9.88(−3)	4.26(−3)	1.07(−3)	1.20(−4)
$4s^{-1}4p^{-1}4d^{+1}4f$	1.04(−3)	9.39(−3)	3.79(−2)	8.93(−2)	1.35(−1)	1.36(−1)	9.18(−2)	3.97(−2)	1.00(−2)
$4d^{-1}5g$	9.77(−4)	7.06(−3)	2.20(−2)	3.80(−2)	3.92(−2)	2.42(−2)	8.25(−3)	1.20(−3)	
$4p^{-1}6p$	8.43(−4)	6.05(−3)	2.05(−2)	3.98(−2)	4.83(−2)	3.75(−2)	1.82(−2)	5.06(−3)	6.14(−4)
$4d^{-1}7d$	8.00(−4)	4.22(−3)	1.19(−2)	1.86(−2)	1.72(−2)	9.18(−3)	2.45(−3)	1.99(−4)	2.49(−5)
$3d^{-2}4f\,5f$	7.36(−4)	3.37(−3)	9.44(−3)	1.73(−2)	2.17(−2)	1.75(−2)	1.12(−2)	4.35(−3)	1.00(−3)
$4p^{-1}4d^{-1}5p\,6d$	6.77(−4)	2.55(−3)	5.87(−3)	8.69(−3)	8.56(−3)	5.62(−3)	2.38(−3)	5.85(−4)	6.41(−5)
$4s^{-1}4d^{-1}5s\,5d$	6.53(−4)	2.69(−3)	6.27(−3)	9.38(−3)	9.35(−3)	6.21(−3)	2.65(−3)	6.59(−4)	7.28(−5)
$3d^{-1}4p^{-1}4d^{+1}4f$	6.46(−4)	5.88(−3)	2.40(−2)	5.73(−2)	8.78(−2)	8.96(−2)	6.09(−2)	2.66(−2)	6.75(−3)
$4d^{-2}4f\,5p$	6.20(−4)	2.19(−3)	4.47(−3)	5.68(−3)	4.62(−3)	2.34(−3)	6.77(−4)	8.56(−5)	
$4p^{-1}4d^{-1}5d\,6p$	5.85(−4)	2.25(−3)	5.20(−3)	7.74(−3)	7.68(−3)	5.08(−3)	2.16(−3)	5.34(−4)	5.88(−5)
$4s^{-1}4d^{-1}4f\,5p$	5.59(−4)	2.26(−3)	5.17(−3)	7.59(−3)	7.42(−3)	4.83(−3)	2.02(−3)	4.93(−4)	5.34(−0)
$4p^{-2}5p^2$	5.30(−4)	2.45(−3)	6.55(−3)	1.15(−2)	1.34(−2)	1.14(−2)	6.53(−3)	2.44(−3)	5.41(−4)
$4d^{-2}5d\,7d$	5.25(−4)	1.50(−3)	2.94(−3)	3.59(−3)	2.81(−3)	1.38(−3)	3.86(−4)	4.72(−5)	
$4s^{-2}4f^2$	4.35(−4)	1.97(−3)	5.32(−3)	9.39(−3)	1.14(−2)	9.57(−3)	5.52(−3)	2.09(−3)	4.68(−4)
$3d^{-1}4d^{-1}4f\,6f$	4.26(−4)	1.56(−3)	3.66(−3)	5.53(−3)	5.58(−3)	3.75(−3)	1.62(−3)	4.08(−4)	4.56(−5)
$4s^{-1}4p^{-1}4f\,5g$	4.09(−4)	1.97(−3)	5.64(−3)	1.06(−2)	1.34(−2)	1.18(−2)	7.12(−3)	2.80(−3)	6.48(−4)
$4s^{-1}4d^{+1}$		3.09(−3)	2.20(−2)	6.71(−2)	1.14(−1)	1.16(−1)	7.05(−2)	2.39(−2)	3.48(−3)
$4s^{-1}5g$	3.04(−4)	2.56(−3)	9.49(−3)	2.00(−2)	2.62(−2)	2.18(−2)	1.13(−2)	3.35(−3)	4.32(−4)
$3d^{-1}4d^{+1}$	4.17(−5)	5.03(−4)	3.59(−3)	1.10(−2)	1.87(−2)	1.90(−2)	1.16(−2)	3.93(−3)	5.71(−4)
$3d^{-1}4p^{-1}4d^{+1}5f$	1.32(−4)	1.32(−4)	1.16(−3)	4.73(−3)	1.72(−2)	1.75(−2)	1.18(−2)	5.12(−3)	1.30(−3)
$4s^{-2}4d^{+2}$		2.84(−4)	2.28(−3)	8.05(−3)	1.62(−2)	2.04(−2)	1.64(−2)	8.27(−3)	2.38(−3)
$4p^{-2}4d^{+1}5g$	6.97(−5)	6.68(−4)	2.87(−3)	7.13(−3)	1.53(−2)	1.19(−2)	8.35(−3)	3.74(−3)	9.75(−4)
$4p^{-1}7p$	2.91(−4)	1.83(−3)	6.16(−3)	1.18(−2)	1.42(−2)	1.10(−2)	5.29(−3)	1.46(−3)	1.76(−4)
$3d^{-2}4d^{+2}$		1.39(−4)	1.12(−3)	3.97(−3)	8.00(−3)	9.14(−3)	8.11(−3)	4.08(−3)	1.17(−3)
$4p^{-2}4d^{+1}5d$	1.04(−4)	9.17(−4)	3.42(−3)	7.41(−3)	1.03(−2)	9.56(−3)	5.89(−3)	2.33(−3)	5.37(−4)
$3d^{-2}4d^{+1}5d$	5.47(−5)	5.07(−4)	2.07(−3)	4.93(−3)	7.53(−3)	6.52(−3)	5.17(−3)	2.25(−3)	5.68(−4)
$3d^{-1}4p^{-1}4d^{+1}5p$	5.16(−5)	4.72(−4)	1.93(−3)	4.60(−3)	7.05(−3)	7.18(−3)	4.87(−3)	2.12(−3)	5.39(−4)
$3d^{-2}4f\,6f$	3.66(−4)	1.57(−3)	4.37(−3)	7.95(−3)	9.90(−3)	8.63(−3)	5.03(−3)	1.95(−3)	4.44(−4)
$3d^{-1}4p^{-1}4d^{+1}6f$	5.72(−5)	4.68(−4)	1.89(−3)	4.44(−3)	6.69(−3)	6.72(−3)	4.49(−3)	1.93(−3)	4.81(−4)
$4s^{-1}4p^{-1}4d^{+1}5p$	6.19(−5)	5.52(−4)	2.15(−3)	4.90(−3)	7.17(−3)	6.99(−3)	4.54(−3)	1.90(−3)	4.62(−4)

1.0×10^{-5}, W^{37+}: 0.0) and therefore it is omitted from our extended CI basis. Note that the CI strength equals zero for the W^{37+} ion because the $4d$ and $5s$ configurations do not interact at all.

Figure 1 demonstrates how CI strength changes for the $4p^6 4d^N$ and $4p^6 4d^{N-2}4f^2$, $4p^4 4d^{N+2}$, $4p^5 4d^N 4f$, $4p^4 4d^N 4f^2$, and $4s4p^5 4d^{N+1}4f$ configurations with the number of electrons, N. The strongest mixing for these configurations is determined near the half-filled d shell, where the number of configuration state functions is the largest.

Squares of the CI expansion coefficients in the atomic wave functions for many levels of $4d^N$ configurations exceed a value of 0.9, which means that mixing with other states is very small. However, for some levels of the $4d^N$ configurations, the

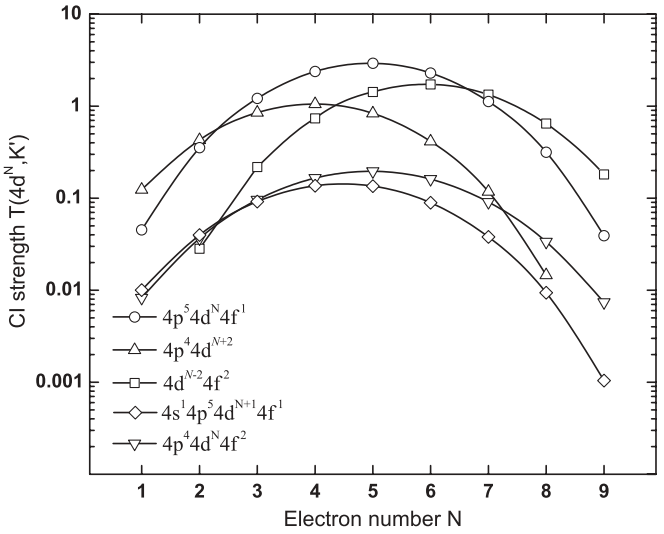

FIG. 1. The CI strength $T(K, K')$ between the $4p^6 4d^{N-2} 4f^2$, $4p^4 4d^{N+2}$, $4p^5 4d^N 4f$, $4p^4 4d^N 4f^2$, and $4s 4p^5 4d^{N+1} 4f$ configurations and the $4d^N$ configuration.

squares of coefficients in the wave-function expansions are close to 0.5 in the *jj*-coupling scheme. Nevertheless, mixing in all cases mainly takes place between the CSFs of the same nonrelativistic configuration.

III. RESULTS AND DISCUSSION

To define the influence of the extended CI basis used in these calculations, we performed calculations of the wavelengths λ and the transition probabilities A using two relativistic codes: FAC and GRASP0. The FAC [6] is based on the Dirac-Fock-Slater approach, whereas the GRASP0 code [7] employs the multiconfiguration Dirac-Fock approximation to determine the transition parameters.

We compared our data with data from the HULLAC calculation performed on the comparatively small basis of six even-parity configurations considered in [3] for the tungsten ions W^{29+} to W^{37+}. Both the calculated and the experimental wavelengths provided in [3] are presented in Table II. Furthermore, data obtained in one-configuration approximation and the results from the largest CI bases used in our calculations are also presented. All our calculations with FAC were performed using the potentials of the ground configurations for corresponding tungsten ions. A large number of magnetic-dipole transitions contribute to the radiative spectrum, especially when the configurations with the half-filled $4d$ shell are considered. CRM was performed in this work to find the strongest lines in the calculated spectrum of magnetic-dipole transitions. The electron-impact excitation cross sections were calculated in the distorted-wave approximation using FAC. The excitation rate coefficients are obtained using the electron beam energies from the EBIT measurements with a Gaussian profile of 30 eV full width at half maximum ($\sigma = 12.74$ eV). The CRM includes the $4d^N$ configuration and the electric dipole coupling of the ground configuration with two excited strongly mixing configurations, namely $4d^{N-1} 4f$ and $4p^5 4d^{N+1}$. Our CRM does not include dielectronic recombination because electron beam energies do not overlap with the resonant energies of dielectronic capture. The ionization process has not been taken into account because its contribution to the lines formed by the radiative cascade has an effect similar to the collisional excitation.

In previous work [3], the CRM was also applied by mixing the ground configuration with the five even-parity configurations ($4p^6 4d^{N-2} 4f^2$, $4p^4 4d^{N+2}$, $4p^5 4d^N 4f$, $4p^4 4d^N 4f^2$, and $4s 4p^5 4d^{N+1} 4f$). In the present study, we have extended the CI basis of even-parity configurations and checked the influence of the $4d^{N-1} np$ and $4d^{N-1} np$ ($n = 5, 6$) configurations. Their effect on the relative intensities of lines is small.

Figure 2 presents our calculated gA values and the line intensities from CRM. The beam energies used in the present CRM calculations are presented in the figure caption and were taken from [3]. It can be seen that the gA values have a much richer structure. However, our set of configurations used in the CRM calculations was not checked for convergence of the line intensities. The larger basis for some ions can significantly change the calculated intensities for some lines, but the size of the rate matrix drastically increases after the inclusion of additional configurations coupled to the considered configurations.

Figure 3 demonstrates how the line intensities for the W^{34+} ion change when two additional (aforementioned) odd-parity configurations are included in the CRM. Here we use a smaller basis of the even-parity configurations for the ion than that in Fig. 2(a), but the same number of transitions that occur inside the ground configuration and between the levels of this configuration and the two odd-parity configurations. Consequently, some wavelengths are different when compared with Fig. 2(a), but only negligible variations of the intensities are observed. The largest increase of the intensity is obtained for the line at $\lambda = 683.74$ Å, which corresponds to the $4d_{3/2}^2(2)\, 4d_{5/2}^2(2)\,(J = 0) \rightarrow 4d_{3/2}^3(3/2)\, 4d_{5/2}(5/2)$ ($J = 1$) transition. The credible explanation for this change is that the calculated population for the ground level with $J = 0$ is several times larger than the population for the excited levels. The electron excitation proceeds mostly to the levels with J values restricted by the dipole-transition selection rules. These are the highly excited levels of the $4d^3\, 4f$ and $4p^5\, 4d^5$ configurations with total angular momenta $J = 0$, 1, which decay back through the electric dipole transitions and mostly populate the levels of $4d^4$ configurations with $J = 0$, 1, 2.

A. W^{29+} and W^{37+} ions

There is only a single line for the $M1$ transitions between two levels of the ground configurations in W^{29+} and W^{37+}. A discrepancy of 1.59 Å exists between the calculated wavelength where the extended CI basis is used and the experimental wavelength for the W^{29+} ion. A smaller discrepancy of 1 Å is determined in HULLAC calculations even when the smaller basis of the six aforementioned configurations is utilized. Our GRASP0 values demonstrate longer wavelengths than those obtained with FAC on the same configuration basis.

The value from the most complex GRASP0 calculation is close to the value of the FAC calculation when the extended CI basis of 34 configurations (in addition to the ground configuration) with the largest CI strengths from Table I is

TABLE II. Comparison of the experimental and theoretical wavelengths (Å) for $M1$ transitions in $4d^N$ ($N = 1, \ldots, 9$) configurations of tungsten. The experimental data (Expt.) and HULLAC calculation results (HULL) are from [3]. Data from the current work are presented for GRASP and FAC calculations within one configuration (CI_1), six configurations (CI_6), and the extended basis (CI_{ext}). N_{ext} is the number of the added configurations, and A is the corresponding radiative transition probability.

Ion	Expt. [3]	HULL [3]	FAC CI_1	GRASP CI_1	FAC CI_6	GRASP CI_6	FAC CI_{ext}	$A(s^{-1})$	N_{ext}	Lower level	Upper level
W^{29+}	756.64	757.6	751.71	758.85	751.99	755.47	755.05	3.72(4)	34	$4d^5_{5/2}$ 5/2	$4d^3_{3/2}$ 3/2
W^{30+}	570.41[a]	570.2	566.36	567.79	569.61	571.06	573.04	1.69(4)	28	$4d^4_{5/2}$ 4	$4d^3_{3/2}(3/2)4d^5_{5/2}(5/2)$ 4
	650.92[a]	666.5	662.79	666.63	665.50	668.01	671.44	6.49(4)	28	$4d^3_{3/2}(3/2)4d^5_{5/2}(5/2)$ 3	$4d^2_{3/2}$ 2
	687.57[a]	712.4	704.82	710.34	708.20	711.46	709.14	2.51(4)	28	$4d^4_{5/2}$ 2	$4d^3_{3/2}(3/2)4d^5_{5/2}(5/2)$ 1
	790.31[a]	785.5	784.22	792.39	783.02	787.71	783.21	2.81(4)	28	$4d^4_{5/2}$ 2	$4d^3_{3/2}$ (3/2)$4d^5_{5/2}(5/2)$ 2
	794.21[a]	790.5	787.07	794.70	785.90	789.90	788.74	4.68(4)	28	$4d^4_{5/2}$ 4	$4d^3_{3/2}(3/2)4d^5_{5/2}(5/2)$ 3
W^{31+}	666.76	664.11	661.17	664.29	661.85	664.04	664.70	3.49(4)	21	$4d^3_{5/2}$ 9/2	$4d^3_{3/2}(3/2)4d^4_{5/2}(4)$ 9/2
	804.88	809.69	799.35	807.20	797.74	801.95	800.22	4.97(4)	21	$4d^3_{5/2}$ 9/2	$4d^3_{3/2}(3/2)4d^4_{5/2}(4)$ 7/2
W^{32+}	661.08[b]	661.9	663.87	666.65	661.64	663.63	664.58	9.20(3)	17	$4d^2_{5/2}$ 4	$4d^3_{3/2}(3/2)4d^3_{5/2}(9/2)$ 5
	668.19	669.4	665.99	672.38	668.19	670.57	670.18	2.18(4)	18	$4d^3_{3/2}(3/2)4d^3_{5/2}(9/2)$ 6	$4d^2_{3/2}(2)4d^4_{5/2}(4)$ 6
	803.03	807.7	807.28	813.23	802.89	806.38	804.44	4.07(4)	21	$4d^2_{5/2}$ 4	$4d^3_{3/2}(3/2)4d^3_{5/2}(9/2)$ 4
		884.6	881.30	891.88	875.82	881.24	879.22	3.18(4)	16	$4d^2_{5/2}$ 4	$4d^3_{3/2}(3/2)4d^3_{5/2}(9/2)$ 3
W^{33+}	692.36	690.9	684.27	687.10	685.77	688.09	691.46	5.57(4)	15	$4d^1_{5/2}$ 5/2	$4d^3_{3/2}(3/2)4d^2_{5/2}(2)$ 3/2
	706.18[b]	706.1	705.34	708.53	703.53	705.87	705.73	2.12(4)	15	$4d^1_{5/2}$ 5/2	$4d^3_{3/2}(3/2)4d^2_{5/2}(4)$ 7/2
	708.22[b]	711.9	709.10	710.35	708.85	711.09	714.38	9.03(4)	15	$4d^3_{3/2}(3/2)4d^2_{5/2}$ (4) 5/2	$4d^2_{3/2}(2)4d^3_{5/2}(9/2)$ 5/2
		993.2	996.31	1000.84	982.94	989.16	980.40	3.90(4)	15	$4d^1_{5/2}$ 5/2	$4d^3_{3/2}(3/2)4d^2_{5/2}(4)$ 5/2
W^{34+}	662.40[b]	656.2	652.47	654.02	654.28	655.99	657.83	6.45(4)	26	$4d^3_{3/2}(3/2)4d^1_{5/2}(5/2)$ 1	$4d^2_{3/2}(2)4d^2_{5/2}(4)$ 2
	680.60[b]	687.6	683.74	687.65	683.74	686.23	690.57	1.23(5)	19	$4d^3_{3/2}(3/2)4d^1_{5/2}(5/2)$ 1	$4d^2_{3/2}(2)4d^2_{5/2}(2)$ 0
	696.95	695.4	691.12	693.75	691.54	693.78	697.96	4.97(4)	26	$4d^3_{3/2}(3/2)4d^1_{5/2}(5/2)$ 2	$4d^2_{3/2}(2)4d^2_{5/2}(2)$ 1
	736.64	739.0	743.26	748.27	737.03	740.09	737.38	2.29(4)	23	$4d^3_{3/2}(3/2)4d^1_{5/2}(5/2)$ 4	$4d^2_{3/2}(2)4d^2_{5/2}(4)$ 5
	855.63[b]	872.5	874.11	883.68	864.11	869.20	863.67	4.08(4)	19	$4d^4_{3/2}$ 0	$4d^3_{3/2}(3/2)4d^1_{5/2}(5/2)$ 1
	864.51[b]	882.7	884.78	894.71	875.43	880.72	875.98	3.70(4)	23	$4d^3_{3/2}(3/2)4d^1_{5/2}(5/2)$ 4	$4d^2_{3/2}(2)4d^2_{5/2}(4)$ 4
W^{35+}		449.38	442.12	466.74	447.90	448.78	450.70	4.83(3)	18	$4d^3_{3/2}$ 3/2	$4d^2_{3/2}(0)4d^1_{5/2}(5/2)$ 5/2
	563.82[b]	565.42	560.26	561.00	564.53	565.77	570.60	3.62(4)	18	$4d^2_{3/2}(2)4d^1_{5/2}(5/2)$ 3/2	$4d^1_{3/2}(3/2)4d^2_{5/2}(4)$ 5/2
	566.54	568.78	563.43	564.59	566.54	567.95	564.86	3.90(4)	18	$4d^2_{3/2}(0)4d^1_{5/2}(5/2)$ 5/2	$4d^1_{3/2}(3/2)4d^2_{5/2}(0)$ 3/2
	615.34[b]	617.66	617.63	619.87	617.25	619.09	616.83	2.19(4)	18	$4d^2_{3/2}(2)4d^1_{5/2}(5/2)$ 9/2	$4d^1_{3/2}(3/2)4d^2_{5/2}(4)$ 11/2
	629.85	630.10	630.18	630.04	627.88	629.94	632.53	6.67(4)	22	$4d^2_{3/2}(2)4d^1_{5/2}(5/2)$ 3/2	$4d^1_{3/2}(3/2)4d^2_{5/2}(2)$ 3/2
	622.30[b]	636.29	627.46	632.54	633.16	635.20	638.17	1.39(4)	20	$4d^3_{3/2}$ 3/2	$4d^2_{3/2}(2)4d^1_{5/2}(5/2)$ 1/2
	659.20[b]	659.70	659.78	662.53	658.80	660.83	660.95	7.27(4)	18	$4d^2_{3/2}(2)4d^1_{5/2}(5/2)$ 5/2	$4d^1_{3/2}(3/2)4d^2_{5/2}(4)$ 7/2
	660.03[b]	660.53	659.98	662.88	658.20	660.47	659.21	6.66(4)	20	$4d^2_{3/2}(2)4d^1_{5/2}(5/2)$ 1/2	$4d^1_{3/2}(3/2)4d^2_{5/2}(2)$ 1/2
	710.46	711.59	706.88	710.51	706.97	709.65	711.17	3.70(4)	22	$4d^3_{3/2}$ 3/2	$4d^2_{3/2}(2)4d^1_{5/2}(5/2)$ 3/2
	756.64[a]	752.74	755.40	760.20	751.04	754.11	749.84	1.95(4)	18	$4d^2_{3/2}(2)4d^1_{5/2}(5/2)$ 7/2	$4d^1_{3/2}(3/2)4d^2_{5/2}(4)$ 9/2
	774.76	775.35	774.43	780.54	771.08	774.79	772.96	3.15(4)	18	$4d^2_{3/2}(2)4d^1_{5/2}(5/2)$ 9/2	$4d^1_{3/2}(3/2)4d^2_{5/2}(4)$ 9/2
	822.68[a]	832.25	836.58	844.10	826.92	831.18	828.71	4.49(4)	18	$4d^3_{3/2}$ 3/2	$4d^2_{3/2}(2)4d^1_{5/2}(5/2)$ 5/2
W^{36+}		450.68	442.07	441.44	450.04	450.54	447.77	1.51(5)	32	$4d^1_{3/2}(3/2)4d^1_{5/2}(5/2)$ 1	$4d^2_{5/2}$ 0
	526.19[a]	526.94	521.17	521.95	525.84	527.03	531.50	1.27(4)	32	$4d^1_{3/2}(3/2)4d^1_{5/2}(5/2)$ 3	$4d^2_{5/2}$ 2
	541.20[b]	547.51	538.35	539.46	544.34	545.75	551.19	3.76(3)	32	$4d^2_{3/2}$ 2	$4d^1_{3/2}(3/2)4d^1_{5/2}(5/2)$ 1
	574.30[b]	580.31	574.62	576.09	578.45	580.00	584.02	2.76(4)	32	$4d^2_{3/2}$ 2	$4d^1_{3/2}(3/2)4d^1_{5/2}(5/2)$ 2
	598.01	593.69	592.61	594.14	593.91	595.45	596.46	5.92(4)	32	$4d^1_{3/2}(3/2)4d^1_{5/2}(5/2)$ 3	$4d^2_{5/2}$ 4
	635.89	633.90	633.19	635.85	632.48	634.57	635.08	4.77(4)	32	$4d^1_{3/2}(3/2)4d^1_{5/2}(5/2)$ 2	$4d^2_{5/2}$ 2
	680.60	678.29	683.95	687.35	679.01	681.35	679.06	2.03(4)	32	$4d^1_{3/2}(3/2)4d^1_{5/2}(5/2)$ 1	$4d^2_{5/2}$ 2
	707.74	712.75	713.86	718.05	710.18	712.96	711.52	5.35(4)	32	$4d^2_{3/2}$ 2	$4d^1_{3/2}(3/2)4d^1_{5/2}(5/2)$ 3
	795.09	798.29	799.41	804.68	794.92	798.36	797.77	1.55(4)	32	$4d^1_{3/2}(3/2)4d^1_{5/2}(5/2)$ 4	$4d^2_{5/2}$ 4
	855.85	854.94	863.64	871.17	850.28	854.64	857.98	2.10(4)	32	$4d^2_{3/2}$ 0	$4d^1_{3/2}(3/2)4d^1_{5/2}(5/2)$ 1
W^{37+}	646.68	650.22	648.05	650.81	645.69	648.22	647.35	3.97(4)	13	$4d^1_{3/2}$ 3/2	$4d^1_{5/2}$ 5/2

[a]Questionable experimental wavelength or line identification in [3].
[b]New identification of line proposed.

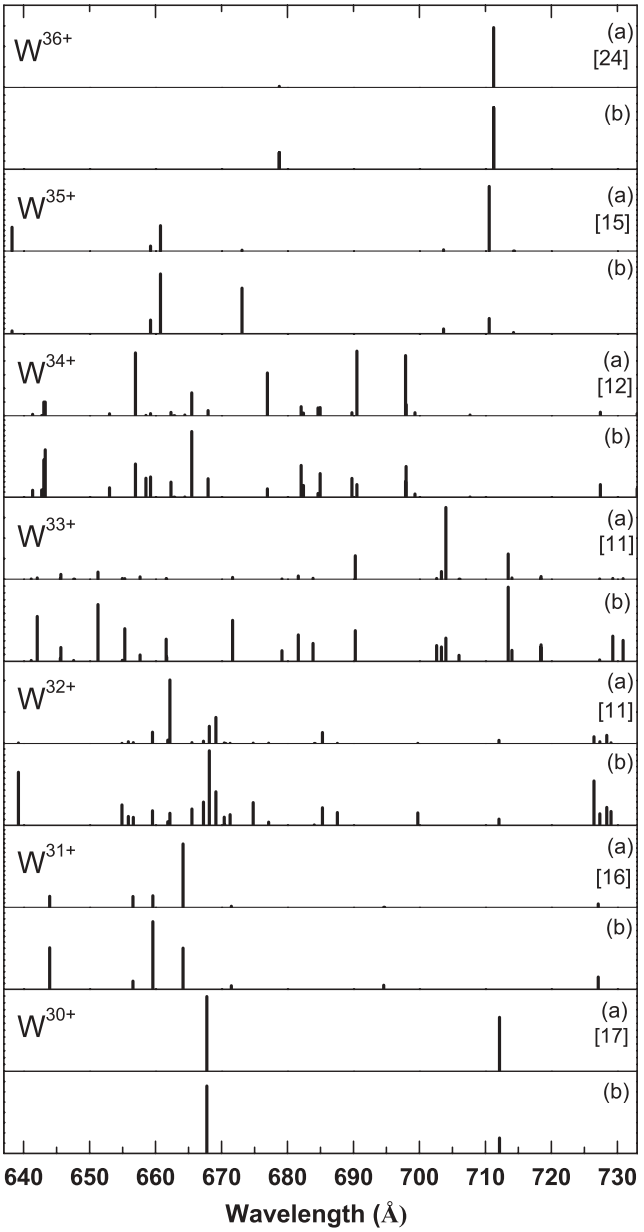

FIG. 2. (a) The line intensities from CRM and (b) gA values of $M1$ transitions. Arbitrary units are used. The numbers of even-parity configurations used in the CI calculations in addition to the ground-state calculation are shown in square brackets. The electric dipole transitions are included in the CRM calculations. The beam energies (in keV) from [3] are W^{30+}, 1.05; W^{31+}, 1.11; W^{32+}, 1.28; W^{33+}, 1.34; W^{34+}, 1.41; W^{35+}, 1.47; and W^{36+}, 1.60.

exploited. In this case the basis consists of 13,572 CSFs. However, we did not include more configurations because our generated set of configurations for the calculations of the CI strength included excitations only up to $n = 7$. Some configurations already have occupied orbitals with this principal quantum number. Therefore, a contribution could arise from the configurations that have orbitals with higher principal quantum numbers and for which the CI strengths were not determined here.

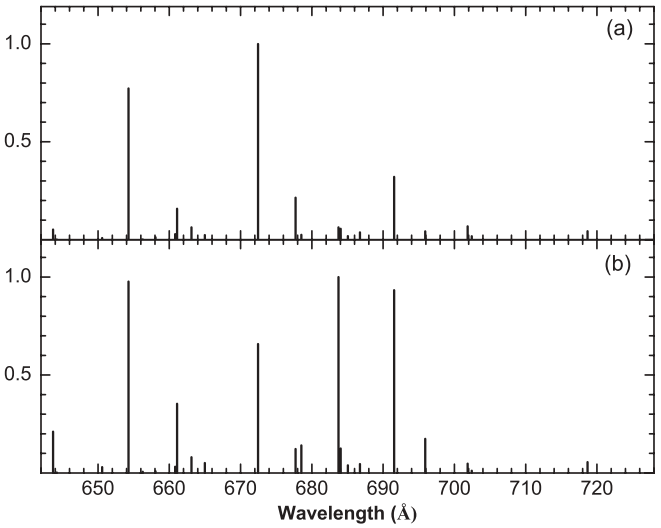

FIG. 3. The CRM line intensities of the $M1$ transitions in W^{34+} calculated (a) when only the transitions among the levels of the $4d^4$ configuration are considered and (b) when $E1$ coupling with two strongly interacting $4p^5 4d^5$ and $4d^3\,4f$ configurations is included.

Significantly better agreement is obtained for the transition wavelength in W^{37+} (i.e., the ion with a higher ionization stage). The deviation of 0.67 Å is determined on the CI basis of 13 configurations with the largest CI strength. Furthermore, the FAC value calculated on the same configuration basis list as in [3] is in better agreement with the measured wavelength than the HULLAC value. It is interesting that, although similar approaches are realized in both codes, the FAC and the HULLAC wavelengths differ by roughly 5 Å for those two ions obtained on the same CI basis of six configurations.

B. W^{30+} ion

The most interesting results are obtained for the ionization stages where the $M1$ transitions originate among more than two levels of ground configurations. More lines appear in the emission spectra, and the identification of these lines requires highly accurate wavelengths and intensities in many cases.

Data obtained with FAC for the W^{30+} ion show that the wavelengths change only by tenths of an angstrom when we continue to expand the basis of interacting configurations (For example, $\lambda = 671.74$ Å for the 26-configuration basis and $\lambda = 671.44$ Å for the 28-configuration basis). Meanwhile, a calculation using only the first 20 configurations from Table I has provided a wavelength value of 668.63 Å. Combining this fact with the small values of CI strength, $T(K, K')$, for the rest of the configurations that are not included in our basis, we infer that further extension of the CI basis would not alter wavelengths by more than 1 Å. We must point out that, referring to the amount of the admixed configurations from Table I used in the calculations, the ground configuration for which the CI strengths are determined is not included. The ground and admixed configurations are taken into account in solving the Hamiltonian matrix.

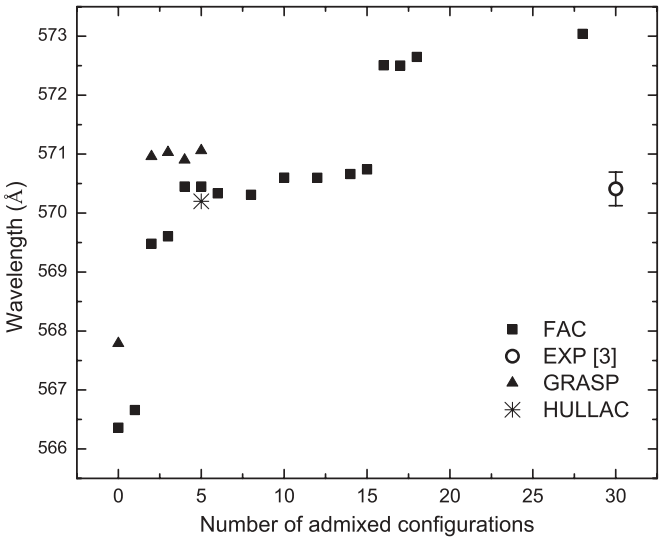

FIG. 4. Dependence of calculated wavelength for the $4d^3_{3/2}(3/2)\ 4d^5_{5/2}(5/2)\ (J=4) \rightarrow 4d^4_{5/2}(4)\ (J=4)$ transition on the number of admixed configurations for the W^{30+} ion.

The same situation is observed for another line: $\lambda = 573.014$ Å on the basis of 20 configurations (plus the ground configuration), $\lambda = 573.036$ Å on the basis of 26 configurations, and $\lambda = 573.041$ Å on the basis of 28 configurations. It reveals that a larger basis would not significantly change the calculated wavelength. However, the discrepancy of approximately 3 Å between our calculated and the experimental results still remains. Furthermore, the value calculated here on the same basis as in the previous work and the one obtained with HULLAC are accidentally close to the experimental value. This fact could explain why this line was assigned to the $4d^3_{3/2}(3/2)\ 4d^5_{5/2}(5/2)\ (J=4) \rightarrow 4d^4_{5/2}(4)\ (J=4)$ transition. Figure 4 demonstrates how the theoretical value of the wavelength changes for this transition when the augmented CI basis from Table I is used. The prominent changes in wavelength values on the figure occur after $4p^5 4d^8 4f$ ($\Delta\lambda = 2.8$ Å) and $4d^7 5g$ ($\Delta\lambda = 1.8$ Å) configurations are added to the CI basis. It should be noted that the CI basis of six configurations used in the HULLAC calculations included the $4d^7 5s$ and $4p^4 4d^{10}$ configurations, whereas more strongly interacting $4p^4 4d^8 5p$ and $4p^4 4d^8 4f^2$ configurations are included in the present CI basis.

Similar convergence is obtained for other three lines: (i) $\lambda = 713.33, 709.12$, and 709.14 Å; (ii) $\lambda = 786.54, 782.99$, and 783.21 Å; (iii) $\lambda = 788.76, 788.77, 788.74$ Å, determined on the basis of 20, 26, and 28 configurations, respectively. In contrast, large discrepancies are observed for these lines when they are compared with proposed experimental identifications. This finding suggests that the values of these wavelengths should be checked using some other methods. However, the peaks in the experimental spectrum [3] for the lines identified from W^{30+} are not strong and there are more observed lines in the spectrum with similar intensities. Therefore, the large theory-experiment deviations most likely are caused by misidentification of the emission lines in the measured spectrum, which has multiple weak features.

C. W^{31+} ion

Two lines for the W^{31+} ion have been calculated, using 21 configurations from Table I. This calculation produced a shift of about 0.3 Å toward the long wavelengths when the two configurations $4d^5 5d^2$ and $4d^6 7d$ were added to the basis of 19 configurations. Therefore, we suppose that the extension of the CI basis should lead to the values closer to the experimentally measured wavelengths. The CI strength for the configurations included in our calculations has larger values compared to the strengths of the W^{30+} ion configuration because a larger number of interacting levels exist.

D. W^{32+} ion

A deviation of about 1.4 Å was determined for the current wavelength on the basis of 21 configurations from the experimental wavelength of 803.03 Å in the W^{32+} ion. A similar difference is obtained for the strong line at $\lambda_{expt} = 668.19$ Å, identified as the $4d^2_{3/2}(2)\,4d^4_{5/2}(4)\ (J=6) \rightarrow 4d^3_{3/2}(3/2)\,4d^3_{5/2}(9/2)\ (J=6)$ transition. Furthermore, the largest discrepancy, more than 3 Å, is observed for the experimental line at $\lambda_{expt} = 661.08$ Å with the previously proposed identification in [3] as the transition between the $4d^3_{3/2}(3/2)4d^3_{5/2}(9/2)\ (J=5)$ and $4d^2_{5/2}\ (J=4)$ levels. Another line produced by the $4d^2_{3/2}(2)4d^4_{5/2}(4)\ (J=6) \rightarrow 4d^3_{3/2}(3/2)4d^3_{5/2}(9/2)\ (J=5)$ transition with a smaller intensity but comparatively large radiative rate of 9.47×10^3 s^{-1} exhibits a better agreement on the CI basis of 17 configurations ($\lambda = 660.17$ Å). We must admit that the calculated intensity of this line is about six times smaller in our CRM than the intensity of the assigned transition. Nevertheless, as mentioned earlier, the configuration basis used here did not ensure that the convergence was reached for the line intensities.

E. W^{33+} ion

For the W^{33+} ion, calculations were limited by the available computer resources; therefore, the largest CI basis only consisted of 15 configurations. Reasonable agreement was accomplished for two lines with the shortest wavelengths presented in Table II. But the strong line with the experimental value $\lambda_{expt} = 708.22$ Å differs by approximately 5 Å from our most elaborate calculation result; therefore, it indicates questionable line identification. Our calculations produce two lines in the vicinity of $\lambda_{expt} = 708.22$ Å with large radiative rates. Thus, the line $\lambda_{expt} = 708.22$ Å corresponds to the $4d^3_{3/2}(3/2)4d^2_{5/2}(4)\ (J=7/2) \rightarrow 4d^1_{5/2}(5/2)\ (J=5/2)$ transition, which has a calculated wavelength equal to 705.73 Å ($A = 2.12 \times 10^4$ s^{-1}) and line $\lambda_{expt} = 706.18$ Å is identified as belonging to the $4d^2_{3/2}(2)4d^3_{5/2}(9/2)\ (J=13/2) \rightarrow 4d^3_{3/2}(3/2)4d^2_{5/2}(4)\ (J=11/2)$ transition with calculated wavelength of 704.49 Å ($A = 7.45 \times 10^3$ s^{-1}). Meanwhile, the FAC calculation on the six-configuration CI basis produces a value that agrees fairly well with this measured intensive line. However, the two lines in Fig. 4 of [3] appear to be wrongly marked on the figure when compared with their tabulated wavelengths ($\lambda_{expt} = 706.18, 708.22$ Å).

F. W^{34+} ion

The strong line observed at $\lambda_{expt} = 662.4$ Å was identified as the $4d^2_{3/2}(2)4d^2_{5/2}(4)$ $(J = 2) \rightarrow 4d^3_{3/2}(3/2)4d^1_{5/2}(5/2)$ $(J = 1)$ transition in the W^{34+} ion in [3]. However, our calculation for the 26-configuration CI basis produces the wavelength value of 657.83 Å, which differs by approximately 4.6 Å. Therefore, this line should be prescribed to the $4d^1_{3/2}(3/2)4d^2_{5/2}(4)$ $(J = 7/2) \rightarrow 4d^2_{3/2}(2)4d^1_{5/2}(5/2)$ $(J = 5/2)$ transition in the W^{35+} ion with calculated wavelength of 660.95 Å. Moreover, this transition has a radiative rate $(A = 7.27 \times 10^4\ s^{-1})$ that is nearly 7 times larger than that proposed earlier [3]. Furthermore, according to the measurements, there is a close-lying line at 659.21 Å with a slightly smaller radiative rate $(A = 6.66 \times 10^4\ s^{-1})$ originating from the $4d^1_{3/2}(3/2)4d^2_{5/2}(2)$ $(J = 1/2) \rightarrow 4d^2_{3/2}(2)4d^1_{5/2}(5/2)$ $(J = 1/2)$ transition in W^{35+}.

The other line that corresponds to the $4d^2_{3/2}(2)\,4d^2_{5/2}(2)$ $(J = 0) \rightarrow 4d^3_{3/2}(3/2)4d^1_{5/2}(5/2)$ $(J = 1)$ transition demonstrates a deviation of roughly 10 Å. The closest candidate for this line is a quite strong line from W^{36+} with calculated wavelength of 679.06 Å, which corresponds to the $4d^2_{5/2}(2)$ $(J = 2) \rightarrow 4d^1_{3/2}(3/2)4d^1_{5/2}(5/2)$ $(J = 1)$ transition.

Significantly better agreement with the experimental values is obtained for the lines $\lambda = 696.95$ Å (for the CI basis of 26 configurations) and $\lambda = 736.64$ Å (for the CI basis of 24 configurations), in which our calculated values are larger by about 1 and 0.7 Å, respectively. The first line has one of the largest values among calculated line intensities but manifests as quite weak in the experimental spectrum, demonstrating that the convergence for the intensities was probably not achieved in the calculations.

One can notice a very large difference between the theoretical wavelengths determined by both the FAC and HULLAC and the experimental data for two lines: $\lambda_{expt} = 855.63$ Å and $\lambda_{expt} = 864.51$ Å. The most striking fact is that, for the transition assigned to the first line in [3], the wavelength value of 863.67 Å is determined after the extension of the CI basis up to 19 configurations in the present calculations. However, when the CI basis of 12 configurations is engaged, a value of 863.46 Å is obtained. Therefore, such behavior confirms that the transition between the two lowest levels of the ground configuration, $4d^3_{3/2}(3/2)\ 4d^1_{5/2}(5/2)$ $(J = 1)$ and $4d^4_{3/2}$ $(J = 0)$, corresponds to the measured line at $\lambda_{expt} = 864.51$ Å but not the line at $\lambda_{expt} = 855.63$ Å. The calculated intensities in the vicinity of the measured wavelength of $\lambda_{expt} = 855.63$ Å are very weak for the W^{33+} and W^{34+} ions, except for the calculated line at $\lambda = 858.56$ Å (the CI basis of 15 configurations) in the W^{35+}, which belongs to the $4d^1_{3/2}(3/2)\ 4d^2_{5/2}(2)$ $(J = 5/2) \rightarrow 4d^2_{3/2}(0)\ 4d^1_{5/2}(5/2)$ $(J = 5/2)$ transition.

G. W^{35+} ion

It seems likely that the line of the W^{35+} ion observed at $\lambda_{expt} = 563.82$ Å is incorrectly identified in the previous work [3]. The large-scale calculations identify the line as the $4d^1_{3/2}(3/2)\ 4d^2_{5/2}(2)$ $(J = 3/2) \rightarrow 4d^2_{3/2}(2)\ 4d^1_{5/2}(5/2)$ $(J = 5/2)$ transition with calculated wavelength of 561.58 Å; $(A = 3.18 \times 10^4\ s^{-1})$. The present FAC calculations for 18 configurations produced the λ value of 570.60 Å for the corresponding line. The identification of two other lines observed at $\lambda_{expt} = 659.2$ Å and $\lambda_{expt} = 660.03$ Å is permuted in [3]. However, even with the large CI basis being employed in the present calculation, the large discrepancy from the experimental measurements for line with $\lambda_{expt} = 622.3$ Å remains. This deviation can be reduced if the line is assigned to the $4d^1_{3/2}(3/2)\ 4d^2_{5/2}(4)$ $(J = 11/2) \rightarrow 4d^2_{3/2}(2)\ 4d^1_{5/2}(5/2)$ $(J = 9/2)$ transition $(\lambda = 616.83$ Å, $A = 2.19 \times 10^4\ s^{-1})$ and $\lambda_{expt} = 615.34$ Å is identified as the $4d^3_{5/2}(9/2)$ $(J = 9/2) \rightarrow 4d^1_{3/2}(3/2)\ 4d^2_{5/2}(4)$ $(J = 7/2)$ transition $(\lambda = 613.66$ Å, $A = 6.24 \times 10^4\ s^{-1})$.

The line observed at $\lambda_{expt} = 710.46$ Å is in sound agreement with the present wavelength value of 711.17 Å $(A = 3.7 \times 10^4\ s^{-1})$ determined on the CI basis of 22 configurations. Additionally, it could belong to or be blended by the transition in the W^{36+} ion $(\lambda = 711.52$ Å, $A = 5.35 \times 10^4\ s^{-1})$. However, the line at 756.64 Å, assigned to the W^{35+} ion in [3], differs peculiarly from our value by about 7 Å. Because the calculated intensity is very weak for this line, the previous identification may be misguided.

Our theoretical value of $\lambda = 772.96$ Å differs by approximately 2 Å from the observed line wavelength; augmenting the CI basis from 15 to 18 configurations has changed the calculated wavelength by 0.8 Å toward better agreement with the experimental value. Unfortunately, reasonable agreement could not be achieved for the measured line at $\lambda_{expt} = 822.68$ Å with a discrepancy of 6 Å. The larger CI basis must be employed to resolve this theory-experiment deviation.

H. W^{36+} ion

For the W^{36+} ion, the very weak line at $\lambda_{expt} = 526.19$ Å differs from our best data by more than 5 Å. The large discrepancies have also been defined for two other lines, $\lambda_{expt} = 541.2$ Å and $\lambda_{expt} = 574.3$ Å. These two lines can be assigned to the transitions in the W^{35+} ion, namely the $4d^1_{3/2}(3/2)\ 4d^2_{5/2}(2)$ $(J = 5/2) \rightarrow 4d^2_{3/2}(2)\ 4d^1_{5/2}(5/2)$ $(J = 7/2)$ transition with $\lambda = 539.87$ Å $(A = 1.89 \times 10^4\ s^{-1})$ and the $4d^1_{3/2}(3/2)\ 4d^2_{5/2}(4)$ $(J = 5/2) \rightarrow 4d^2_{3/2}(2)\ 4d^1_{5/2}(5/2)$ $(J = 3/2)$ transition with $\lambda = 570.6$ Å $(A = 3.62 \times 10^4\ s^{-1})$. Even the calculation using the 18-configuration CI basis does not ensure satisfactory agreement with the experimental wavelength values. Other calculated wavelengths for this ion are in better agreement with observed values.

IV. CONCLUSIONS

To critically evaluate previous line identifications, detailed comparisons with a recent experiment were performed for the wavelengths of the magnetic dipole transitions between the levels of $4d^N$ configurations in multicharged tungsten ions. New interpretations of some lines have been proposed that allowed the large theory-experiment deviations that

existed in the previous data to be removed. The accuracy of the current results is better than 0.5% for most wavelengths.

The CI strengths $T(K, K')$ for the $4d^N$ configurations have been determined to define the set of configurations which have the largest interaction with the ground configuration. Large-scale calculations were performed for magnetic dipole transitions to check the previous line identification. The analysis of magnetic dipole transitions in the $4d^N$ configurations for tungsten ions has confirmed that the large CI basis must be used to achieve substantial agreement with the experimental measurements of wavelengths. The convergence of the agreement of calculated and measured wavelengths has been achieved for most lines, whereas for some transitions, especially in W^{33+} and W^{34+} ions, the larger CI basis must be used to ensure convergence.

ACKNOWLEDGMENTS

This work was partly supported by the European Communities under the contract of association between EURATOM and the Lithuanian Energy Institute. It was carried out within the framework of the European Fusion Development Agreement and partly funded by the European Commission, Project No. RI026715 (BalticGrid), and also by the Lithuanian State Science and Studies Foundation in the frame of the projects LitGrid and GridTechno. We also wish to thank an anonymous referee for thoughtful and constructive comments.

[1] A. Kallenbach, R. Neu, R. Dux, H. U. Fahrbach, J. Fuchs, L. Giannone, O. Gruber, A. Herrmann, P. Lang, B. Lipschultz, C. F. Maggi, J. Neuhauser, V. Philipps, T. Putterich, V. Rohde, J. Roth, G. Sergienko, and A. Sips (ASDEX Upgrade Team), Plasma Phys. **47**, B207 (2005).

[2] R. Radtke, C. Biedermann, P. Mandelbaum, and J. L. Schwob, J. Phys. **58**, 113 (2007).

[3] R. Radtke, C. Biedermann, G. Fussmann, J. Schwob, P. Mandelbaum, and R. Doron, in *Atomic and Plasma-Material Interaction Data for Fusion* (International Atomic Energy Agency, Vienna, 2007), Vol. 13, p. 45.

[4] A. Bar-Shalom, M. Klapisch, and J. Oreg, J. Quant. Spectrosc. Radiat. Transfer **71**, 169 (2001).

[5] http://sprg.ssl.berkeley.edu/∼mfgu/fac/.

[6] M. F. Gu, Astrophys. J. **582**, 1241 (2003).

[7] I. P. Grant, B. J. McKenzie, P. H. Norrington, D. F. Mayers, and N. C. Pyper, Comput. Phys. Commun. **21**, 207 (1980).

[8] Y. Ralchenko, J. N. Tan, J. D. Gillaspy, J. M. Pomeroy, and E. Silver, Phys. Rev. A **74**, 042514 (2006).

[9] Y. Ralchenko, J. Reader, J. M. Pomeroy, J. N. Tan, and J. D. Gillaspy, J. Phys. B **40**, 3861 (2007).

[10] Y. Ralchenko, I. N. Draganic, J. N. Tan, J. D. Gillaspy, J. M. Pomeroy, J. Reader, U. Feldman, and G. E. Holland, J. Phys. B **41**, 021003 (2008).

[11] T. Pütterich, R. Neu, C. Biedermann, R. Radtke, and ASDEX Upgrade Team, J. Phys. B **38**, 3071 (2005).

[12] V. Jonauskas, S. Kučas, and R. Karazija, J. Phys. B **40**, 2179 (2007).

[13] R. Karazija, *Sums of Atomic Quantities and Mean Characteristics of Spectra* (Mokslas, Vilnius, Lithuania, 1991).

[14] S. Kučas and R. Karazija, Phys. Scripta **47**, 754 (1993).

[15] S. Kučas, V. Jonauskas, and R. Karazija, Phys. Scripta **55**, 667 (1997).

[16] V. Jonauskas, S. Kučas, and R. Karazija, Phys. Scripta **67**, 208 (2003).

[17] S. Kučas, V. Jonauskas, R. Karazija, and I. Martinson, Phys. Scripta **51**, 566 (1995).

[18] S. Kučas, R. Karazija, V. Jonauskas, and S. Aksela, Phys. Scripta **52**, 639 (1995).

[19] V. Jonauskas, S. Kučas, R. Karazija, and P. H. Norrington, Phys. Scripta **75**, 237 (2007).

[20] J. Bauche, C. Bauche-Arnoult, M. P. Klapisch Mandelbaum, and J. L. Schwob, J. Phys. B **20**, 1443 (1987).

[21] R. Karazija, *Introduction to the Theory of X-Ray and Electronic Spectra of Free Atoms* (Plenum Press, New York, 1996).

[22] F. A. Parpia, C. Froese Fischer, and I. P. Grant, Comput. Phys. Commun. **94**, 249 (1996).

[23] S. Kučas, V. Jonauskas, R. Karazija, and A. Momkauskaitė, Lithuan. J. Phys. **47**, 249 (2007).

[24] R. Radtke, C. Biedermann, J. L. Schwob, P. Mandelbaum, and R. Doron, Phys. Rev. A **64**, 012720 (2001).

[25] J. Jimenez-Mier, D. L. Ederer, T. Schuler, and T. A. Callcott, J. Phys. B **36**, L173 (2003).

[26] R. Karpuškienė, R. Karazija, and P. Bogdanovich, Phys. Scripta **64**, 333 (2001).